ISSN 1063-7761, Journal of Experimental and Theoretical Physics, 2017, Vol. 124, No. 3, pp. 388–405. © Pleiades Publishing, Inc., 2017.
Original Russian Text © V.A. Loiko, A.V. Konkolovich, V.Ya. Zyryanov, A.A. Miskevich, 2017, published in Zhurnal Eksperimental'noi i Teoreticheskoi Fiziki, 2017, Vol. 151, No. 3, pp. 457–475.

ATOMS, MOLECULES, OPTICS

Small-Angle Light Scattering Symmetry Breaking in Polymer-Dispersed Liquid Crystal Films with Inhomogeneous Electrically Controlled Interface Anchoring

V. A. Loiko[a]*, A. V. Konkolovich[a], V. Ya. Zyryanov[b], and A. A. Miskevich[a]

[a] *Stepanov Institute of Physics, National Academy of Sciences of Belarus, Minsk, 220072 Belarus*
[b] *Kirensky Institute of Physics, Federal Research Center "Krasnoyarsk Scientific Center," Siberian Branch, Russian Academy of Sciences, Kraskoyarsk, 660036 Russia*
**e-mail: loiko@ifanbel.bas-net.by*

Received August 16, 2016

Abstract—We have described the method of analyzing and reporting on the results of calculation of the small-angle structure of radiation scattered by a polymer-dispersed liquid crystal film with electrically controlled interfacial anchoring. The method is based on the interference approximation of the wave scattering theory and the hard disk model. Scattering from an individual liquid crystal droplet has been described using the anomalous diffraction approximation extended to the case of droplets with uniform and nonuniform interface anchoring at the droplet–polymer boundary. The director field structure in an individual droplet is determined from the solution of the problem of minimizing the volume density of the free energy. The electrooptical effect of symmetry breaking in the angular distribution of scattered radiation has been analyzed. This effect means that the intensities of radiation scattered within angles $+\theta_s$ and $-\theta_s$ relative to the direction of illumination in the scattering plane can be different. The effect is of the interference origin and is associated with asymmetry of the phase shift of the wavefront of an incident wave from individual parts of the droplet, which appears due to asymmetry of the director field structure in the droplet, caused by nonuniform anchoring of liquid crystal molecules with the polymer on its surface. This effect is analyzed in the case of normal illumination of the film depending on the interfacial anchoring at the liquid crystal–polymer interface, the orientation of the optical axes of droplets, their concentration, sizes, anisometry, and polydispersity.

DOI: 10.1134/S1063776117020133

1. INTRODUCTION

Theoretical and experimental investigations of polymer-dispersed liquid-crystal (PDLC) films are of considerable interest owing to their application in display systems, as well as systems for optical information processing, telecommunication, optoelectronics, etc. [1–5]. These films can form the basis for multifunctional devices with tunable characteristics, such as optical radiation intensity and phase modulators, polarizers, light polarization transformers, lenses, filters, reflectors, and flexible displays [6–13].

Liquid-crystal (LC) droplets in PDLC films are dispersed in a binding polymer matrix. The intrinsic orientational structure of droplets varies under the action of external electric or magnetic fields. No additional polaroids are required for the formation of the optical response in light-scattering media in contrast to traditionally used homogeneous LCs in the birefringence mode. Polymer films with dispersed LC droplets exhibit flexibility, high mechanical strength, optical strength, and are distinguished by simple fabrication technique.

The following two approaches to the control over the optical response of PDLC films in the light-scattering mode are known at present.

The first approach is based on the classical Freedericksz effect [14–17]. The essence of this effect is that the orientation of LC molecules in the entire bulk of LC droplets is changed by an external controlling field. The anchoring between LC molecules and the polymer matrix remains unchanged. After the removal of the field, the intrinsic orientational structure of LC droplets returns to the initial state due to elastic interaction forces in the liquid crystal. The classical Freedericksz effect forms the basis of modern electrooptical LC systems.

An new approach to controlling the structure of LC droplets [18] in a polymer matrix has been proposed and implemented recently using the local Freedericksz transition [19, 20], in which the orientation of the director in the bulk of an LC droplet changes due to the competing action of various surface forces in a small near-surface region. This method is based on a modification of the boundary conditions at the LC–

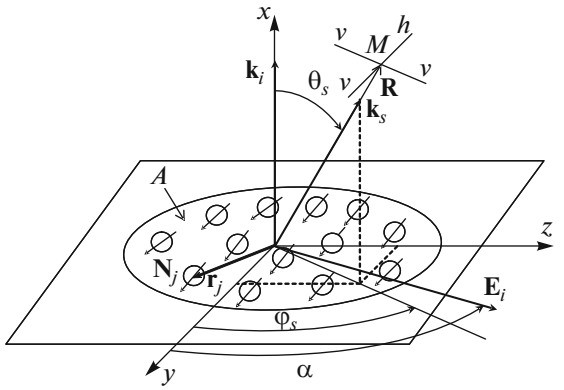

Fig. 1. Schematic representation of the geometry of illumination of a PDLC monolayer: *xyz* is the laboratory system of coordinates; *x* is the direction of propagation of the incident wave; *yz* is the plane of the monolayer; $\mathbf{k}_i$, $\mathbf{E}_i$, and α are the wavevector, polarization vector, and polarization angle of the incident wave, respectively; $\mathbf{k}_s$, θ_s, and φ_s are the wavevector, scattering angle, and angle of orientation of scattering plane ($\mathbf{k}_i$, $\mathbf{k}_s$), respectively; lines *vv* and *vh* define the directions of the polarization vector components of the scattered wave parallel and perpendicular to polarization plane ($\mathbf{E}_i$, $\mathbf{k}_i$) of the incident wave; $\mathbf{N}_j$ is the director of an individual droplet, whose position in the monolayer is determined by radius vector $\mathbf{r}_j$; *A* is the area of the layer under investigation; **R** is the radius vector of point of observation *M*.

polymer interface by ion-forming surfactants (surface-active substances). An ion surfactor produces nonuniformity in the anchoring on surface of droplets and makes it possible to substantially (by orders of magnitude) reduce the strengths of controlling electric field as compared to PDLC materials exhibiting uniform anchoring.

In an analysis of the electrooptical response in PDLC films with nonuniform interfacial anchoring and for constructing the models that describe the effects of electrically controlled light scattering, it is necessary to take into account the optical anisotropy of LCs, the orientational structure of LC molecules in droplets (which depends on the anchoring at the interface and changes under the action of the external controlling field), the concentration of LC droplets and surfactant, the properties of the polymer matrix, multiple scattering of light, and other parameters.

No rigorous theory of light scattering by dispersed optically anisotropic media (including PDLC materials) has been developed. For this reason, approximate methods are employed [21–26]. In this study, we are using the interference approximation of the theory of wave scattering for describing light scattering in PDLC layers with nonuniform interfacial anchoring at the droplet–polymer boundary (Section 2). We consider multilayer films. Section 3 contains the relations that describe the spatial distribution of polydisperse ensembles of droplets, which are based on the hard disk model and the substitution model. The approximation of anomalous diffraction for analyzing light scattering by an individual droplet with uniform and nonuniform anchoring in a polymer matrix is described in Section 4. A method for solving the problem of minimizing the volume density of free energy, which is used to determine the internal structure of the field of the director (local optical axes) of droplets, is described in Section 5. Section 6 contains the results of a comparison of the theoretical and experimental data on the angular structure of scattered light in PDLC monolayers. Small-angle scattering of light by an individual LC droplet and by monolayer PDLC films is considered in Section 7. We conduct a detailed analysis of the electrooptical effect of breaking symmetry in the small-angle distribution of scattered radiation in films with inhomogeneous boundary conditions of the tangentially normal type. The essence of this effect is that the values of intensity of radiation scattered into angles $+\theta_s$ and $-\theta_s$ relative to the illumination direction in the scattering plane (defined by the wavevectors of the incident and scattered waves) can be different [27–29]. It should be noted that films with a uniform surface anchoring are characterized by a symmetric distribution of the intensity of radiation scattered into angles $+\theta_s$ and $-\theta_s$ [1, 2, 27–29].

2. INTERFERENCE APPROXIMATION FOR DESCRIBING LIGHT SCATTERING IN A MONOLAYER PDLC FILM

Let us consider a PDLC monolayer illuminated by a linearly polarized plane wave along the normal (Fig. 1). The director $\mathbf{N}_j$ of an individual droplet ($j = 1, 2, ..., N$, where N is the number of droplets in the layer) characterizes the direction of orientation of longer axes of LC molecules, averaged over the droplet volume. Let us suppose that the layer is formed by an ensemble of polydisperse LC droplets having the shape of spheres or spheroids with different circular sections in the *yz* plane of the layer. We assume that LC droplets do not penetrate into one another. We will analyze the *vv* and *vh* components of scattered light, which are polarized parallel and perpendicular to the polarization plane ($\mathbf{E}_i$, $\mathbf{k}_i$) of incident wave, respectively. In the experiment, the *vv* and *vh* components are measured in parallel and crossed polarizer and analyzer, respectively.

We consider the scattering geometry in which scattering angle θ_s can vary from $-\pi$ to π, and angle φ_s of orientation of the scattering plane varies in the range of $0-\pi$.

For a disperse layer with small difference between the refractive indices of LC and of the polymer matrix, the mutual reradiation of LC droplets, i.e., multiple light scattering, is negligibly weak, and we can use the single scattering approximation also known as the interference approximation [30] because it takes into account the interference of waves singly scattered by

droplets in the far field zone. Then, we can write the following relations for the vv and vh components of scattered field, $E^s_{vv}(\mathbf{R})$ and $E^s_{vh}(\mathbf{R})$, at point of observation M with radius vector $\mathbf{R}$, which is in the far wave zone [30, 31]:

$$E^s_{vv,vh}(\mathbf{R}) = \sum_{j=1}^{N} E_j^{vv,vh}(\mathbf{R})\exp(-i\mathbf{k}_s\cdot\mathbf{r}_j) = \sum_{l=1}^{m} E_l^{vv,vh}(\mathbf{R})\sum_{j=1}^{N_l}\exp(-i\mathbf{k}_s\cdot\mathbf{r}_j^l), \quad (1)$$

where $E_j^{vv,vh}(\mathbf{R})$ are the field components at point M scattered by the jth droplet, $\mathbf{r}_j$ is the radius vector to its center in the yz plane of the monolayer; l is the type of droplets, which depends on the areas of cross sections of LC droplets by the yz plane of the monolayer; m is the total number of distinguishable types of droplets; and N_l is the number of l-type droplets. In expression (1), scattered field components $E_l^{vv,vh}(\mathbf{R})$ for each type l of droplets have the form

$$E_l^{vv,vh}(\mathbf{R}) = f_l^{vv,vh}(\mathbf{k}_s)\frac{iE_i}{kR}\exp(ikR), \quad (2)$$

where $f_l^{vv,vh}(\mathbf{k}_s)$ are the vv and vh components of the vector amplitude scattering function [30, 32] in the direction of scattering wavevector $\mathbf{k}_s$ for an individual droplet of the l type, E_i is the amplitude of the incident wave, $k = 2\pi n_p/\lambda$, n_p is the refractive index of the binding polymer matrix, and λ is the wavelength of light.

For intensity components I_{vv} and I_{vh} of scattered radiation corresponding to the vv and vh polarizations, we can write

$$I_{vv,vh} = \langle|E^s_{vv,vh}(\mathbf{R})|^2\rangle, \quad (3)$$

where the angle brackets denote averaging over the positions of LC droplets in the layer.

Relations (1) and (2) imply that

$$|E^s_{vv,vh}(\mathbf{R})|^2 = \frac{|E_i|^2}{k^2R^2}\sum_{l,l'=1}^{m} f_l^{vv,vh}(\mathbf{k}_s)f_{l'}^{vv^*,vh^*}(\mathbf{k}_s) \times\sum_{j=1}^{N_l}\sum_{k=1}^{N_{l'}}\exp[-ik_s\cdot(\mathbf{r}_j^l-\mathbf{r}_k^{l'})], \quad (4)$$

where the symbol "*" indicates complex conjugation of the components of the vector amplitude scattering function. Separating the terms with $j = k$ and $l = l'$ in the last expression and averaging over the positions of LC droplets in the layer, we obtain

$$\langle|E^s_{vv,vh}(\mathbf{R})|^2\rangle = \frac{|E_i|^2}{k^2R^2}N\sum_{l=1}^{m}P_l|f_l^{vv,vh}(\mathbf{k}_s)|^2 + \frac{|E_i|^2}{k^2R^2}\sum_{l,l'=1}^{m} f_l^{vv,vh}(\mathbf{k}_s)f_{l'}^{vv^*,vh^*}(\mathbf{k}_s) \times\left\langle\sum_{\substack{j=1\\ j\neq i}}^{N_l}\sum_{\substack{i=1\\ l\neq l'}}^{N_{l'}}\exp[-i\mathbf{k}_s\cdot(\mathbf{r}_j^l-\mathbf{r}_i^{l'})]\right\rangle. \quad (5)$$

The second term of this expression describes interference of light scattered from the ensemble of LC droplets in the far field zone.

The extent of the manifestation of the interference effects depends on the mean value of the double sum enclosed in the angle brackets in expression (5). We can write it in the form [30, 33, 34]

$$\left\langle\sum_{\substack{j=1\\ j\neq i}}^{N_l}\sum_{\substack{i=1\\ l\neq l'}}^{N_{l'}}\exp[-i\mathbf{k}_s\cdot(\mathbf{r}_j^l-\mathbf{r}_i^{l'})]\right\rangle = N^2P_lP_{l'}\int_A\int_A W_{ll'}(\mathbf{r}_i^{l'},\mathbf{r}_j^l)\exp[i\mathbf{k}_s\cdot(\mathbf{r}_i^{l'}-\mathbf{r}_j^l)]\frac{d\mathbf{r}_j^l}{A}\frac{d\mathbf{r}_i^{l'}}{A}. \quad (6)$$

Here, $W_{ll'}(\mathbf{r}_i^{l'}, \mathbf{r}_j^l)$ are partial binary (two-particle) distribution functions [35, 36] characterizing the probability of detecting droplets of the l and l' types with coordinates of their centers at the points defined by radius vectors $\mathbf{r}_j^l$ and $\mathbf{r}_i^{l'}$; $P_l = N_l/N$ is the partial fraction of LC droplets of the l type, and $\sum_{l=1}^{m}P_l = 1$. Substituting expression (6) into (5) and separating the vv and vh components I^c_{vv} and I^c_{vh} of coherently scattered light, which are defined in terms of the mean field [30, 34] ($I^c_{vv,vh} = |\langle E^s_{vv,vh}(\mathbf{R})\rangle|^2$), we obtain the following expression for the second term in expression (5):

$$\frac{|E_i|^2}{k^2R^2}\sum_{l,l'=1}^{m} f_l^{vv,vh}(\mathbf{k}_s)f_{l'}^{vv^*,vh^*}(\mathbf{k}_s) \times\left\langle\sum_{\substack{j=1\\ j\neq i}}^{N_l}\sum_{\substack{i=1\\ l\neq l'}}^{N_{l'}}\exp[-i\mathbf{k}_s\cdot(\mathbf{r}_j^l-\mathbf{r}_i^{l'})]\right\rangle = \frac{|E_i|^2N^2}{k^2R^2}\sum_{l,l'=1}^{m}P_lP_{l'}f_l^{vv,vh}(\mathbf{k}_s)f_{l'}^{vv^*,vh^*}(\mathbf{k}_s) \times\int_A\int_A[W_{ll'}(\mathbf{r}_i^{l'},\mathbf{r}_j^l)-1]\exp[i\mathbf{k}_s\cdot(\mathbf{r}_i^{l'}-\mathbf{r}_j^l)] \times\frac{d\mathbf{r}_j^l}{A}\frac{d\mathbf{r}_i^{l'}}{A}+|\langle E^s_{vv,vh}(\mathbf{R})\rangle|^2. \quad (7)$$

Considering that the spatial arrangement of LC droplets is statistically homogeneous and isotropic (functions $W_{ll'}(\mathbf{r}_i^{l'}, \mathbf{r}_j^{l})$ depend only on the modulus of the difference of vectors $\mathbf{r}_i^{l'} - \mathbf{r}_j^{l}$), we obtain the following expression from formulas (4)–(7) for the intensity components I_{vv} and I_{vh} of light scattered by the PDLC monolayer (expression (3)):

$$I_{vv,vh} = I^{c}_{vv,vh} + I^{\text{inc}}_{vv,vh}. \tag{8}$$

In this relation,

$$I^{\text{inc}}_{vv,vh} = \frac{|E_i|^2}{k^2R^2} N \sum_{l=1}^{m} P_l |f_l^{vv,vh}(\mathbf{k}_s)|^2 + \frac{|E_i|^2}{k^2R^2} N \sum_{l,l'=1}^{m} P_l P_{l'} f_l^{vv,vh}(\mathbf{k}_s) f_{l'}^{vv*,vh*}(\mathbf{k}_s)[S'_{ll'}(\mathbf{k}_s) - 1] \tag{9}$$

are the intensity components of incoherently (diffusely) scattered light and functions $S'_{ll'}(\mathbf{k}_s)$ are partial structure factors of the form [35]

$$S'_{ll'}(\mathbf{k}_s) = 1 + \Lambda \int_A [W_{ll'}(r) - 1] \exp(i\mathbf{k}_s \cdot \mathbf{r}) d\mathbf{r}, \tag{10}$$

where $\Lambda = N/A$ is the number density of droplets per unit area, $\mathbf{r} = \mathbf{r}_i^{l'} - \mathbf{r}_j^{l}$, $r = |\mathbf{r}|$, and $W_{ll'}(r)$ are partial radial distribution functions. These functions characterize the conditional probability of detecting LC droplets of various types at distance r in the yz plane of the monolayer in contract to expressions (6) and (7), in which quantities $W_{ll'}(\mathbf{r}_i^{l'}, \mathbf{r}_j^{l})$ characterize the probability of simultaneous location of two LC droplets of types l and l' at points with coordinates $\mathbf{r}_j^{l}$ and $\mathbf{r}_i^{l'}$.

The average-field components that determine the vv and vh components $I^{c}_{vv,vh}$ of the coherent part of the scattered radiation intensity in expression (8) have the form

$$\langle E^{s}_{vv,vh}(\mathbf{R}) \rangle = \frac{iE_i}{kR} \exp(ikR) \sum_{l=1}^{m} f_l^{vv,vh}(\mathbf{k}_s) \frac{N_l}{A} \times \int_A \exp(-i\mathbf{k}_s \cdot \mathbf{r}) d\mathbf{r}, \tag{11}$$

where the integrals over surface A differ from zero, as shown in [30, 34], in the directions close to the direction of light incidence ($\mathbf{k}_s = \mathbf{k}_i$) within the angle of diffraction divergence of the beam in directions close to the strictly backward direction ($\mathbf{k}_s = -\mathbf{k}_i$). It should be noted that, by taking into account the diffraction field of the incident wave on contour A, using relations (11), we can obtain the amplitude transmittances $T^{a}_{vv,vh}$ and reflectances $R^{a}_{vv,vh}$ of the PDLC monolayer for the vv and vh average-field components [30, 34] as follows:

$$T^{a}_{vv} = 1 - \frac{N}{A} \sum_{l=1}^{m} \frac{\lambda}{k} P_l f_l^{vv}(\mathbf{k}_s = \mathbf{k}_i), \tag{12}$$

$$T^{a}_{vh} = -\frac{N}{A} \sum_{l=1}^{m} \frac{\lambda}{k} P_l f_l^{vh}(\mathbf{k}_s = \mathbf{k}_i), \tag{13}$$

$$R^{a}_{vv,vh} = -\frac{N}{A} \sum_{l=1}^{m} \frac{\lambda}{k} P_l f_l^{vv,vh}(\mathbf{k}_s = -\mathbf{k}_i). \tag{14}$$

It can be seen from relations (9) and (10) that, to analyze the angular distribution of the scattered radiation intensity, we must determine components $f_l^{vv}(\mathbf{k}_s)$ and $f_l^{vh}(\mathbf{k}_s)$ of the vector amplitude scattering function for an ensemble of LC droplets of various types l, as well as the partial radial distribution functions $W_{ll'}(r)$ and corresponding partial structural factors $S'_{ll'}(\mathbf{k}_s)$. In the general case, the solution of the problem of scattering by a monolayer is complicated and cumbersome in view of the complexity of solution of the problem of scattering by an individual LC droplet upon a change in the configuration of LC molecules in a droplet under the action of external factors, as well as the complexity in the description of the spatial distribution of LC droplets of various sizes in the PDLC monolayer (see Sections 3 and 4).

For applications, it is convenient to transform relation (9) into the equivalent relation

$$I^{\text{inc}}_{vv,vh} = \frac{|E_i|^2 N}{k^2R^2} \sum_{l,l'=1}^{m} (P_l P_{l'})^{1/2} f_l^{vv,vh}(\mathbf{k}_s) f_{l'}^{vv*,vh*}(\mathbf{k}_s) \times \left\{ \delta_{ll'} + (\Lambda_l \Lambda_{l'})^{1/2} \int_A [W_{ll'}(r) - 1] \exp(i\mathbf{k}_s \cdot \mathbf{r}) d\mathbf{r} \right\}, \tag{15}$$

where $\delta_{ll'}$ are the Kronecker deltas ($\delta_{ll'} = 1$ for $l = l'$ and $\delta_{ll'} = 0$ for $l \neq l'$), Λ_l and $\Lambda_{l'}$ are partial number densities of droplets of the l and l' types per unit area, and $\sum_{l=1}^{m} \Lambda_l = \Lambda$. The structural factors in expression (15) are defined as follows [37]:

$$S_{ll'}(\mathbf{k}_s) = \delta_{ll'} + (\Lambda_l \Lambda_{l'})^{1/2} \int_A [W_{ll'}(r) - 1] \exp(i\mathbf{k}_s \cdot \mathbf{r}) d\mathbf{r}. \tag{16}$$

Then, the relations for $I^{\text{inc}}_{vv,vh}$ assume the form

$$I^{\text{inc}}_{vv,vh} = \frac{|E_i|^2 N}{k^2R^2} \sum_{l,l'=1}^{m} (P_l P_{l'})^{1/2} f_l^{vv,vh}(\mathbf{k}_s) f_{l'}^{vv*,vh*}(\mathbf{k}_s) S_{ll'}(\mathbf{k}_s). \tag{17}$$

Comparison with Eq. (9) shows that this expression has a more visual form, which is convenient for calculations.

The partial structural factors determined with the help of relation (16) can be obtained (see Section 3) from the solution of the generalized Ornstein–Zernike equation [38–40]. Partial structural factors (10) and (16) are related as follows:

$$S'_{ll'}(\mathbf{k}_s) = 1 + \frac{\Lambda}{(\Lambda_l\Lambda_{l'})^{1/2}}[S_{ll'}(\mathbf{k}_s) - \delta_{ll'}]. \quad (18)$$

Concluding the section, we note that expressions (9), (10) (or (16), (17)) can be used to describe the angular structure of scattered light and for 3D PDLC films. In this case, the partial radial distribution functions $W_{ll'}(r)$ describe an ensemble of LC droplets in the 3D space. Then, we must evaluate the integrals in expressions (10) and (16) over volume V instead of integrating over surface A. In this case, Λ, Λ_l, and $\Lambda_{l'}$ denote the number density and partial densities of droplets per unit volume V.

3. ANALYTIC SOLUTIONS OF SCATTERING PROBLEM: HARD DISK MODEL AND SUBSTITUTION MODEL

In this section, we will obtain an analytic solution to the problem of radiation scattering by monolayer PDLC films containing polydisperse spherical or spheroidal LC droplets with circular cross sections in the yz plane of the monolayer. We will use the hard disk model [37, 41] and the substitution model [35, 42, 43]. In determining partial structural factors $S_{ll'}(\mathbf{k}_s)$ (relation (16)), different types l and l' of LC droplets correspond to different values of radii c_l and $c_{l'}$ of their cross section by the monolayer plane.

To determine the partial structural factors, we write the generalized Ornstein–Zernike equation [38]

$$H_{ll'}(r) = C_{ll'}(r) + \sum_{\gamma=1}^{m}\Lambda_\gamma\int_A C_{l\gamma}(r)H_{\gamma l'}(|\mathbf{r} - \mathbf{r}_1|)d\mathbf{r}_1, \quad (19)$$

where $H_{ll'}(r) = W_{ll'}(r) - 1$ is the total correlation function for each type of l and l' pairs of LC droplets; $l, l' = 1, 2, \ldots, m$, and $C_{ll'}(r)$ is the direct correlation function. Multiplying the left- and right-hand sides of Eq. (19) by $(\Lambda_l\Lambda_{l'})^{1/2}$ and performing the Fourier transformation taking into account the fact that it contains integrals of the convolution type, we find that

$$\hat{\tilde{H}}(\mathbf{k}_s) = \hat{\tilde{C}}(\mathbf{k}_s) + \hat{\tilde{C}}(\mathbf{k}_s)\hat{\tilde{H}}(\mathbf{k}_s), \quad (20)$$

where the tilde denotes the matrices of size $m \times m$. Their elements are functions $\tilde{H}_{ll'}(\mathbf{k}_s)$ and $\tilde{C}_{ll'}(\mathbf{k}_s)$ defined in terms of 2D Fourier transforms as follows:

$$\tilde{H}_{ll'}(\mathbf{k}_s) = (\Lambda_l\Lambda_{l'})^{1/2}\int_A [W_{ll'}(r) - 1]\exp(i\mathbf{k}_s\cdot\mathbf{r})d\mathbf{r}, \quad (21)$$

$$\tilde{C}_{ll'}(\mathbf{k}_s) = (\Lambda_l\Lambda_{l'})^{1/2}\int_A C_{ll'}(r)\exp(i\mathbf{k}_s\cdot\mathbf{r})d\mathbf{r}. \quad (22)$$

Let us write expression (20) in the equivalent form

$$\hat{I} + \hat{\tilde{H}}(\mathbf{k}_s) = \hat{I} + \hat{\tilde{C}}(\mathbf{k}_s) + \hat{\tilde{C}}(\mathbf{k}_s)[\hat{I} + \hat{\tilde{H}}(\mathbf{k}_s) - \hat{I}]. \quad (23)$$

Then, relations (16) and (21) yield

$$\hat{S}(\mathbf{k}_s) = \hat{I} + \hat{\tilde{C}}(\mathbf{k}_s) + \hat{\tilde{C}}(\mathbf{k}_s)[\hat{S}(\mathbf{k}_s) - \hat{I}], \quad (24)$$

where $\hat{I}$ is the unit $m \times m$ matrix and $\hat{S}(\mathbf{k}_s)$ is the matrix of partial structural factors $S_{ll'}(\mathbf{k}_s)$.

Relation (24) shows that partial structural factors $S_{ll'}(\mathbf{k}_s)$ are defined by the matrix relation

$$\hat{S}(\mathbf{k}_s) = [\hat{I} - \hat{\tilde{C}}(\mathbf{k}_s)]^{-1}. \quad (25)$$

Consequently, if we know functions $\tilde{C}_{ll'}(\mathbf{k}_s)$ defined in terms of Fourier transforms (relation (22)) of direct partial correlation functions $C_{ll'}(r)$, relation (25) allows us to define matrix $\hat{S}(\mathbf{k}_s)$ of partial structural factors $S_{ll'}(\mathbf{k}_s)$ introduced in accordance with definition (16).

Using the analytic approximation for the 2D Fourier transforms of direct correlation functions [37], which was obtained using the Percus–Yevick approximation [35] for hard circular disks located on the plane, we can write

$$\tilde{C}_{ll'}(\mathbf{k}_s) = (\Lambda_l\Lambda_{l'})^{1/2}\tilde{c}_{ll'}(\mathbf{k}_s), \quad (26)$$

where

$$\begin{aligned}-\tilde{c}_{ll'}(\mathbf{k}_s) = {}& \chi^{(2)}\pi c_l^2\frac{2J_1(k\sin\theta_s c_l)}{k\sin\theta_s c_l}\pi c_{l'}^2\frac{2J_1(k\sin\theta_s c_{l'})}{k\sin\theta_s c_{l'}}\\ &+\chi^{(1)}\left[2\pi c_l\cdot 2J_0(k\sin\theta_s c_l)\pi c_{l'}^2\frac{2J_1(k\sin\theta_s c_{l'})}{k\sin\theta_s c_{l'}}\right.\\ &\left.+2\pi c_{l'}\cdot 2J_0(k\sin\theta_s c_{l'})\pi c_l^2\frac{2J_1(k\sin\theta_s c_l)}{k\sin\theta_s c_l}\right]\\ &+\chi^{(0)}\left[\pi(c_l + c_{l'})^2\frac{2J_1(k\sin\theta_s(c_l + c_{l'}))}{k\sin\theta_s(c_l + c_{l'})}\right].\end{aligned} \quad (27)$$

In the latter relation, J_0 and J_1 are cylindrical first-kind Bessel functions of the zeroth and first order, respectively,

$$\chi^{(0)} = \left(1 - \sum_{l=1}^{m}\Lambda_l\pi c_l^2\right)^{-1}, \quad (28)$$

$$\chi^{(1)} = \frac{1}{2\pi}\left(\sum_{l=1}^{m}\Lambda_l 2\pi c_l\right)\left(1 - \sum_{l=1}^{m}\Lambda_l\pi c_l^2\right)^{-2}, \quad (29)$$

$$\chi^{(2)} = \Lambda\left(1-\sum_{l=1}^{m}\Lambda_l\pi c_l^2\right)^{-2} + \frac{1}{2\pi}\left(\sum_{l=1}^{m}\Lambda_l 2\pi c_2\right)^2 \times\left(1-\sum_{l=1}^{m}\Lambda_l\pi c_l^2\right)^{-3}. \quad (30)$$

It can be seen from relations (25)–(30) that partial structural factors $S_{ll'}(\mathbf{k}_s)$ in the model of hard disks for a monolayer with spherical or spheroidal droplets depend only on scattering angle θ_s. They are independent of angle φ_s of orientation of the scattering plane and are determined by the sizes of LC droplets (c_l and $c_{l'}$), partial number densities of droplets (Λ_l and $\Lambda_{l'}$), and number density Λ of droplets, which characterizes their total number per unit area.

In the above-described analytic model of hard disks, the angular structure of radiation scattered by a monolayer of polydisperse droplets can be determined using relations (16), (17), and (25)–(30).

To calculate the angular distribution of the intensity of light scattered by the PDLC monolayer of monodisperse LC droplets with the oriented structure of their optical axes $\mathbf{N}_j$, we must set $c_l = c_{l'} = c$ in expressions (27)–(30), where c is the radius of the cross section σ of droplets, $\sigma = \pi c^2$. Then, from relations (27)–(30), we obtain the following familiar expression [41] for structural factor $S(\theta_s)$ for a monolayer of monodisperse spherical droplets as follows:

$$S(\theta_s) = \left[1+\frac{4\eta}{1-\eta}\frac{2J_1(2u)}{2u}+\frac{4\eta^2}{(1-\eta)^2}J_0(u)\frac{2J_1(u)}{u} + \left(\frac{\eta^2}{(1-\eta)^2}+\frac{2\eta^3}{(1-\eta)^3}\right)\left(\frac{2J_1(u)}{u}\right)^2\right]^{-1}, \quad (31)$$

where $u = kc\sin\theta_s$, $\eta = N\sigma/A$ is the filling factor for the PDLC monolayer, which is equal to the ratio of the cross section of droplets by the monolayer plane to the area over which these droplets are distributed. This gives the following expression for scattered light intensity components $I^{\text{inc}}_{vv,vh}$:

$$I^{\text{inc}}_{vv,vh}(\theta_s,\varphi_s) = C\frac{\eta}{\sigma k^2}|f_{vv,vh}(\theta_s,\varphi_s)|^2 S(\theta_s). \quad (32)$$

Here, $C = AE_i^2/R^2$ is the normalization constant, and components $f_{vv,\,vh}(\theta_s, \varphi_s)$ of the vector amplitude scattering functions are defined in terms of amplitude scattering matrix elements [21, 30, 43] $S_j, j = 1, 2, 3, 4$ as follows:

$$f_{vv}(\theta_s,\varphi_s) = S_2(\theta_s,\varphi_s)\cos^2(\alpha-\varphi_s) + S_1(\theta_s,\varphi_s)\sin^2(\alpha-\varphi_2) + \frac{1}{2}[S_3(\theta_s,\varphi_s)+S_4(\theta_s,\varphi_s)]\sin[2(a-\varphi_s)], \quad (33)$$

$$f_{vh}(\theta_s,\varphi_s) = S_3(\theta_s,\varphi_s)\sin^2(\alpha-\varphi_s) - S_4(\theta_s,\varphi_s)\cos^2(\alpha-\varphi_s) + \frac{1}{2}[S_2(\theta_s,\varphi_s)-S_1(\theta_s,\varphi_s)]\sin[2(a-\varphi_s)]. \quad (34)$$

In these relations, α (see Fig. 1) is the polarization angle of incident light (angle between polarization vector $\mathbf{E}_i$ of the incident wave and the y axis along which optical axes $\mathbf{N}_j$ of LC droplets are oriented).

It should be noted that, according to the results of calculations [30, 34, 35], analytic formulas (27), (31) in the hard disk model yield admissible results for the layer filling factor $\eta \le 0.5$–0.6.

With a layer filling factor of $\eta \le 0.4$, the analysis of the angular structure of light scattered by the PDLC monolayer can be carried out using the substitution model [35, 42–44]. It presumes that the transposition of any two droplets does not change the spatial configuration of the entire ensemble, but imposes certain limitations on the concentration of droplets in the layer and their polydispersity.

In the substitution model, for partial structural factors $S'_{ll'}(\mathbf{k}_s)$ (relation (10), we must assume that

$$S'_{ll'}(\mathbf{k}_s) \approx S_m(\theta_s), \quad (35)$$

where $S_m(\theta_s)$ is the value of structural factor (31) averaged over the radius c of LC droplets. On the basis of relation (9), we can then obtain the following expression for the vv and vh components of intensity of radiation incoherently scattered by a monolayer of LC droplets [43]:

$$I^{\text{inc}}_{vv,vh}(\theta_s,\varphi_s) = C\frac{\eta}{\langle\sigma\rangle k^2}[\langle|f_{vv,vh}(\theta_s,\varphi_s)|^2\rangle - |\langle f_{vv,vh}(\theta_s,\varphi_s)\rangle|^2(S_m(\theta_s)-1)], \quad (36)$$

where $\langle\sigma\rangle$ is the mean value of the section of droplets by the monolayer plane, the filling factor is $\eta = N\langle\sigma\rangle/A$, and angle brackets indicate averaging over the sizes of LC droplets and the orientations of their optical axes.

Assuming that the internal structure of droplets is the same and their optical axes $\mathbf{N}_j$ lie in the yz plane of the layer and are distributed uniformly over orientation angles φ_d relative to the y axis of the laboratory system of coordinates, we obtain the following expressions for the mean values of the vector amplitude function components and the squares of their moduli appearing in relation (36):

$$\langle f_{vv}(\theta_s,\varphi_s)\rangle = \langle S_2(\theta_s,\varphi_s)\rangle\overline{\cos^2(\alpha-\varphi_s-\varphi_d)} + \langle S_1(\theta_s,\varphi_s)\rangle\overline{\sin^2(\alpha-\varphi_s-\varphi_d)} + \frac{1}{2}\langle[S_3(\theta_s,\varphi_s)+S_4(\theta_s,\varphi_s)]\rangle\overline{\sin[2(\alpha-\varphi_s-\varphi_d)]}, \quad (37)$$

$$\langle f_{vh}(\theta_s,\varphi_s)\rangle = \langle S_3(\theta_s,\varphi_s)\rangle\overline{\sin^2(\alpha-\varphi_s-\varphi_d)} - \langle S_4(\theta_s,\varphi_s)\rangle\overline{\cos^2(\alpha-\varphi_s-\varphi_d)} + \frac{1}{2}\langle[S_2(\theta_s,\varphi_s)-S_1(\theta_s,\varphi_s)]\rangle\overline{\sin[2(\alpha-\varphi_s-\varphi_d)]}, \quad (38)$$

$$\begin{aligned}\langle|f_{vv}|^2\rangle &= \langle|S_2|^2\rangle\overline{\cos^4(\alpha-\varphi_s-\varphi_d)} + \langle|S_1|^2\rangle\overline{\sin^4(\alpha-\varphi_s-\varphi_d)} \\ &+\frac{1}{4}\langle[S_1S_2^* + S_2S_1^* + (S_3+S_4)(S_3^*+S_4^*)]\rangle \\ &\times\overline{\sin^2[2(\alpha-\varphi_s-\varphi_d)]} \\ &+\frac{1}{8}\langle[(S_3+S_4)S_2^* + S_2(S_3^*+S_4^*)]\rangle \\ &\times\{\overline{2\sin[2(\alpha-\varphi_s-\varphi_d)]} + \overline{\sin[4(\alpha-\varphi_s-\varphi_d)]}\} \\ &+\frac{1}{8}\langle[(S_3+S_4)S_1^* + S_1(S_3^*+S_4^*)]\rangle \\ &\times\{\overline{2\sin[2(\alpha-\varphi_s-\varphi_d)]} - \overline{\sin[4(\alpha-\varphi_s-\varphi_d)]}\},\end{aligned} \quad (39)$$

$$\begin{aligned}\langle|f_{vh}|^2\rangle &= \langle|S_3|^2\rangle\overline{\sin^4(\alpha-\varphi_s-\varphi_d)} + \langle|S_4|^2\rangle\overline{\cos^4(\alpha-\varphi_s-\varphi_d)} \\ &+\frac{1}{4}\langle[(S_2-S_1)(S_2^*-S_1^*) - S_4S_3^* - S_3S_4^*]\rangle \\ &\times\overline{\sin^2[2(\alpha-\varphi_s-\varphi_d)]} \\ &-\frac{1}{8}\langle[(S_2-S_1)S_4^* + S_4(S_2^*-S_1^*)]\rangle \\ &\times\{\overline{2\sin[2(\alpha-\varphi_s-\varphi_d)]} + \overline{\sin[4(\alpha-\varphi_s-\varphi_d)]}\} \\ &+\frac{1}{8}\langle[(S_2-S_1)S_3^* + S_3(S_2^*-S_1^*)]\rangle \\ &\times\{\overline{2\sin[2(\alpha-\varphi_s-\varphi_d)]} - \overline{\sin[4(\alpha-\varphi_s-\varphi_d)]}\}.\end{aligned} \quad (40)$$

Here, the bar over expressions indicates averaging over azimuthal angle φ_d, and angle brackets on the right-hand sides indicate averaging over radius c of the cross section of the LC droplet.

In relations (37)–(40), we have

$$\overline{\cos^2(\alpha-\varphi_s-\varphi_d)} = \frac{1}{2}\{1+\cos[2(\alpha-\varphi_s)]\operatorname{sinc}(2\varphi_m)\}, \quad (41)$$

$$\overline{\sin^2(\alpha-\varphi_s-\varphi_d)} = \frac{1}{2}\{1-\cos[2(\alpha-\varphi_s)]\operatorname{sinc}(2\varphi_m)\}, \quad (42)$$

$$\overline{\sin[2(\alpha-\varphi_s-\varphi_d)]} = \sin[2(\alpha-\varphi_s)]\operatorname{sinc}(2\varphi_m), \quad (43)$$

$$\overline{\cos^4(\alpha-\varphi_s-\varphi_d)} = \frac{3}{8}+\frac{1}{2}\cos[2(\alpha-\varphi_s)]\operatorname{sinc}(2\varphi_m) + \frac{1}{8}\cos[4(\alpha-\varphi_s)]\operatorname{sinc}(4\varphi_m), \quad (44)$$

$$\overline{\sin^4(\alpha-\varphi_s-\varphi_d)} = \frac{3}{8}-\frac{1}{2}\cos[2(\alpha-\varphi_s)]\operatorname{sinc}(2\varphi_m) + \frac{1}{8}\cos[4(\alpha-\varphi_s)]\operatorname{sinc}(4\varphi_m), \quad (45)$$

$$\overline{\sin^2[2(\alpha-\varphi_s-\varphi_d)]} = \frac{1}{2}\{1-\cos[4(\alpha-\varphi_s)]\operatorname{sinc}(4\varphi_m)\}, \quad (46)$$

$$\overline{\sin[4(\alpha-\varphi_s-\varphi_d)]} = \sin[4(\alpha-\varphi_s)]\operatorname{sinc}(4\varphi_m), \quad (47)$$

where φ_m is the maximal azimuthal angle of deviation of optical axes of droplets relative to the y axis of the laboratory system of coordinates and $\operatorname{sinc}(x) = \sin(x)/x$. The optical axes of the droplets are oriented along the y axis for $\varphi_m = 0$ and at random for $\varphi_m = \pi$. For $0 < \varphi_m < \pi$, the optical axes of the droplets are oriented partly. Relations (41)–(47) characterize the orientational structure of the PDLC monolayer.

The substitution model (relations (36)–(47)) makes it possible to analyze the angular distribution of the intensity of radiation scattered by monolayer PDLC films depending on the optical characteristics of droplets, their concentration, polydispersity, and orientation of the optical axes. For this purpose, we must determine elements S_j (j = 1, 2, 3, 4) of the amplitude scattering matrix that appear in relations (37)–(40) and average them over the sizes of LC droplets.

4. ANOMALOUS DIFFRACTION APPROXIMATION: SMALL-ANGLE SCATTERING OF LIGHT BY LC DROPLET WITH ARBITRARY INTERNAL STRUCTURE

In this section, we describe the anomalous diffraction approximation [45] as applied to the determination of the amplitude scattering matrix for a spheroidal optically anisotropic LC droplet with an arbitrary internal structure [27]. This approximation makes it possible to analyze the characteristics of radiation scattered by an optically soft large LC droplet into small angles determined by the relation $2kc\sin^2(\theta_s/2) < 0.5$ [46].

Using the anomalous diffraction approximation, we determine the scattered light field in the far-field zone as a result of diffraction by a plane amplitude–phase screen, which approximates a scatterer, with a complex transmittance matrix defined on the projection of the scatterer onto the plane orthogonal to the direction of light incidence [22, 45].

Let us suppose that a droplet is illuminated along the x axis (Fig. 2). Using the results obtained in [47],

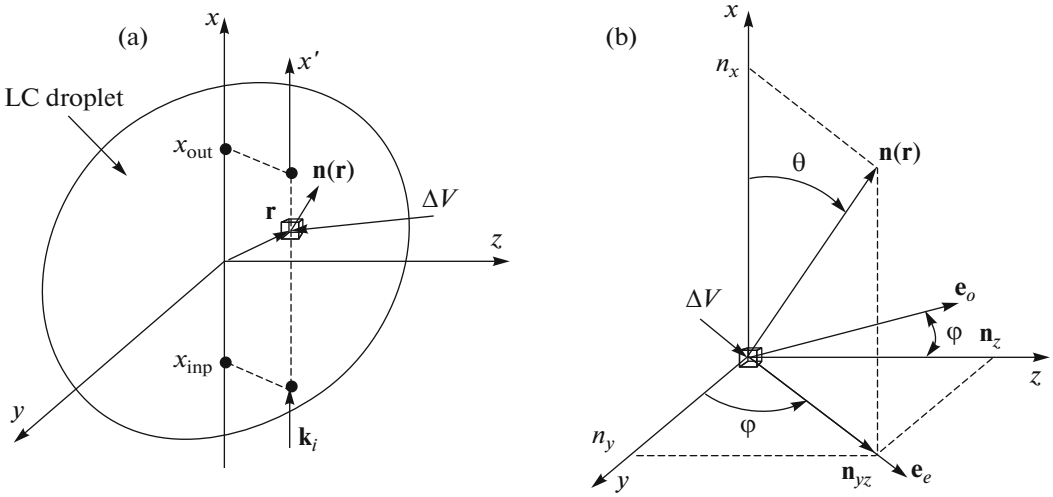

Fig. 2. Schematic representation of (a) an LC droplet and (b) its volume element ΔV: $\mathbf{n}(\mathbf{r})$ is the local director of volume elements ΔV at the point with radius vector $\mathbf{r}$; x_{inp} and x_{out} are the input and output coordinates of the wavefront on the surface of the LC droplet; $\mathbf{k}_i$ is the wavevector of the incident wave; θ and φ are the polar and azimuthal angles of orientation of local director $\mathbf{n}(\mathbf{r})$; $\mathbf{e}_o$ and $\mathbf{e}_e$ are the unit vectors of polarization of the ordinary and extraordinary waves in volume element ΔV; n_x, n_y, and n_z are the Cartesian coordinates of local director $\mathbf{n}(\mathbf{r})$.

we can write the following expressions for amplitude scattering matrix elements S_j (j = 1, 2, 3, 4):

$$S_1(\theta_s,\varphi_s)=\frac{k^2\sigma}{2\pi}\int\limits_{\sigma}[1-T_1(y,z)]\times\exp[-i(ky\cos\varphi_s+kz\sin\varphi_s)\sin\theta_s]dydz, \quad (48)$$

$$S_2(\theta_s,\varphi_s)=\frac{k^2\sigma}{2\pi}\cos\theta_s\int\limits_{\sigma}[1-T_2(y,z)]\times\exp[-i(ky\cos\varphi_s+kz\sin\varphi_s)\sin\theta_s]dydz, \quad (49)$$

$$S_3(\theta_s,\varphi_s)=-\frac{k^2\sigma}{2\pi}\cos\theta_s\int\limits_{\sigma}T_3(y,z)\times\exp[-i(ky\cos\varphi_s+kz\sin\varphi_s)\sin\theta_s]dydz, \quad (50)$$

$$S_4(\theta_s,\varphi_s)=-\frac{k^2\sigma}{2\pi}\int\limits_{\sigma}T_4(y,z)\times\exp[-i(ky\cos\varphi_s+kz\sin\varphi_s)\sin\theta_s]dydz, \quad (51)$$

where $\hat{T}$ is the 2 × 2 Jones matrix [48, 49] of the equivalent amplitude–phase screen.

Jones matrix $\hat{T}$ depends on the internal structure of LC droplets and is defined as [26, 27, 44]

$$\hat{T}(y,z)=\begin{pmatrix}T_2(y,z) & T_3(y,z)\\ T_4(y,z) & T_1(y,z)\end{pmatrix}=\prod_{x=x_{\text{inp}}(y,z)}^{x=x_{\text{out}}(y,z)}R^T(x)PR(x), \quad (52)$$

where

$$x_{\text{inp}}=-\varepsilon a\sqrt{1-(y^2+z^2)/c^2},$$

$$x_{\text{out}}=+\varepsilon a\sqrt{1-(y^2+z^2)/c^2}$$

are the input and output coordinates of the wave front on the LC droplet surface (Fig. 2a); ε is the anisometry parameter equal to the ratio of the semiminor axis a of the droplet (along the x axis) to the semimajor axis c (in the yz plane); $\varepsilon = a/c$ ($\varepsilon = 1$ for spheres); P is the matrix determined by local phase shifts for the extraordinary and ordinary waves, $R(x)$ and $R^T(x)$ are the matrices of coordinate transformations over the tract of local bases;

$$P=\begin{pmatrix}\exp[ik(n_e(\mathbf{r})/n_p-1)\Delta x] & 0\\ 0 & \exp[ik(n_o/n_p-1)\Delta x]\end{pmatrix}, \quad (53)$$

$$R(x)=\begin{pmatrix}\cos[\varphi(\mathbf{r})-\varphi_s] & -\sin[\varphi(\mathbf{r})-\varphi_s]\\ \sin[\varphi(\mathbf{r})-\varphi_s] & \cos[\varphi(\mathbf{r})-\varphi_s]\end{pmatrix}, \quad (54)$$

$$R^T(x)=\begin{pmatrix}\cos[\varphi(\mathbf{r})-\varphi_s] & \sin[\varphi(\mathbf{r})-\varphi_s]\\ -\sin[\varphi(\mathbf{r})-\varphi_s] & \cos[\varphi(\mathbf{r})-\varphi_s]\end{pmatrix}, \quad (55)$$

$n_e(\mathbf{r})$ is the local refractive index of volume element ΔV at the point with radius vector $\mathbf{r}$ for the extraordinary wave, the direction of the polarization vector of which is determined by unit vector $\mathbf{e}_e$ (see Fig. 2b); n_o is the local refractive index for the ordinary wave, which is polarized along unit vector $\mathbf{e}_o$, is independent of coordinates x, y, z, and is equal to refractive index $n_\perp$ for the ordinary wave in the LC; Δx is the longitudinal size of volume element ΔV of a droplet along the direction of illumination, within which the orientational structure of LC local director $\mathbf{n}(\mathbf{r})$ is assumed to be homogeneous and determined by only the molecular order

parameter [1, 2]; and $\varphi(\mathbf{r})$ is the azimuthal angle of orientation of the local principal plane

$$n_e(\mathbf{r}) = \frac{n_\parallel n_\perp}{\sqrt{n_\parallel^2 \cos^2\theta(\mathbf{r}) + n_\perp^2 \sin^2\theta(\mathbf{r})}} = \frac{n_\parallel n_\perp}{\sqrt{n_\parallel^2 n_x^2 + n_\perp^2(1-n_x^2)}}, \quad (56)$$

$$\cos[\varphi(\mathbf{r}) - \varphi_s] = (n_y \cos\varphi_s + n_z \sin\varphi_s)/\sqrt{1-n_x^2}, \quad (57)$$

$$\sin[\varphi(\mathbf{r}) - \varphi_s] = (n_z \cos\varphi_s - n_y \sin\varphi_s)/\sqrt{1-n_x^2}. \quad (58)$$

In these expressions, $\theta(\mathbf{r})$ is the polar angle of the orientation of local director $\mathbf{n}(\mathbf{r})$ (see Fig. 2); $n_\parallel$ is the refractive index for the extraordinary wave in the LC; and n_x, n_y, and n_z are the Cartesian components of local director $\mathbf{n}(\mathbf{r})$ at the point with radius vector $\mathbf{r}$.

Relations (48)–(58) make it possible to analyze small-angle light scattering by LC droplets with an arbitrary structure of the vector field of local director $\mathbf{n}(\mathbf{r})$ in the bulk of an LC droplet. The method of determining the distribution of field director $\mathbf{n}(\mathbf{r})$ will be described in the next section.

5. CALCULATION OF DIRECTOR FIELD CONFIGURATION

The distribution of the field director in a LC droplet is determined by the following factors [2, 15]: (i) the balance between the intermolecular interaction in the LC, which leads to molecules ordering typical of the given LC phase; (ii) the interaction with the polymer, which leads to the orientation of LC molecules along the boundaries of the droplet (tangential boundary conditions) or perpendicularly to them (normal boundary conditions) depending on the interfacial boundary conditions on the surfaces of droplets; and (iii) the external electric (or magnetic) field applied to the PDLC film, which orients the LC molecules. Molecules in an LC droplet are oriented so as to ensure the free energy minimum.

We calculate the orientational ordering of local director $\mathbf{n}(\mathbf{r})$ in the bulk of an LC droplet of a nematic using the procedure of minimization of free energy density F. In the single-constant approximation [1, 2, 28, 50–52], we have

$$F = F_{\text{el}} + F_e, \quad (59)$$

where F_{el} is the elastic deformation energy density,

$$F_{\text{el}} = \frac{1}{2} K[(\text{div}\mathbf{n}(\mathbf{r}))^2 + (\text{curl}\mathbf{n}(\mathbf{r}))^2], \quad (60)$$

and

$$F_e = \frac{1}{2}\varepsilon(\mathbf{E}\cdot\mathbf{n}(\mathbf{r}))^2 \quad (61)$$

is the free energy density associated with the action of the external control electric field with field strength vector $\mathbf{E}$.

In relations (60) and (61), K is the mean value of the elastic modulus, $\varepsilon = \varepsilon_0\Delta\varepsilon$, $\varepsilon_0 = 8.85 \times 10^{-12}$ C^2/(N m^2) is the electric constant, and $\Delta\varepsilon$ is the dielectric anisotropy of the LC.

In calculating the orientational structure of LC droplets with nonuniform surface anchoring, we can disregard the electric contribution to free energy density F_e [53, 54] due to the screening of external control field $\mathbf{E}$ by spatially separated surfactant ions. Using expression (60), we obtain the following relation for the distribution of local director $\mathbf{n}(\mathbf{r})$ corresponding to the free energy density minimum:

$$K\Delta\mathbf{n}(\mathbf{r}) = 0. \quad (62)$$

Here, Δ is the Laplace operator.

For solving Eq. (62) and for determining components n_x, n_y, and n_z of local director $\mathbf{n}(\mathbf{r})$ in the Cartesian system of coordinates, we have used the difference scheme of calculations [26]. The technique for calculating the internal orientational structure of an LC droplet involves the following procedures:

(i) first, a certain (initial) orientation of the director in the bulk of the droplet is specified;

(ii) the volume of the droplet is divided into cells, and the orientation of local director $\mathbf{n} = \mathbf{n}(\mathbf{r})$ is determined;

(iii) the iteration procedure (relaxation method) is used, in which the orientation of the longer axes of molecules in the LC droplet is directed along the normal (normal boundary conditions) and along the tangent (tangential boundary condition) to the surface.

Figure 3 shows the schematics of the section of a spheroidal LC droplet by a plane perpendicular to the plane of the layer. To quantitatively estimate the degree of nonuniformity of surface anchoring of the LC with the polymer matrix, we use parameter w (see Fig. 3). It characterizes the size of the region of the droplet with normal surface anchoring. It should be noted that the values of $w = 0\%$ and 100% correspond to uniform surface anchoring on the LC–polymer interface. For $w = 0\%$, only tangential anchoring takes place, and a bipolar LC configuration is formed in the droplet. For $w = 100\%$, only normal anchoring occurs, and the internal orientational structure of the droplet is radial. For other values of w, the LC configuration in the droplet is more complex [28, 53, 54].

Parameter w depends on the internal control field [26]. Its variations lead to change in the internal structure of droplets and, accordingly, in their optical characteristics, as well as the characteristics of the entire PDLC layer. As noted above, the field in a droplet is equal to zero due to screening by the surfactant. Optical axis $\mathbf{N}$ of a droplet (see Fig. 3) is perpendicular to the surface that divides the droplet into regions with

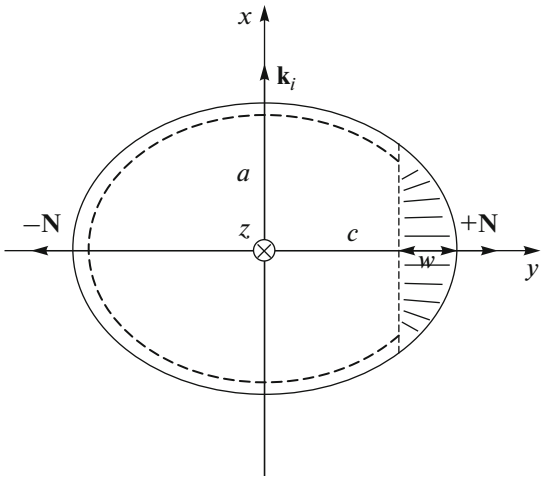

Fig. 3. Schematic diagram of the section of an LC droplet with nonuniform anchoring by the *xy* plane. Parameter *w* characterizes the fraction of the droplet surface with normal (homeotropic) anchoring; *a* and *c* are the semiminor and semimajor axes of the droplet; **N** is the optical axis of the droplet; and $\mathbf{k}_i$ is the wavevector of the incident wave. Dashed curve shows the orientation of the longer axes of LC molecules on the droplet surface (along the normal and along the tangent).

different anchorings of LC molecules with the polymer. The +**N** and −**N** directions are nonequivalent because regions of the droplet with different anchorings are determined by the direction of the control electric field vector **E**. To reverse the orientation of the optical axis of the droplet, we must change the polarity of the control field.

It should be noted that the +**N** and −**N** directions for an LC droplet with uniform tangential surface anchoring and with the bipolar configuration of the local director are equivalent [2]. It should also be noted that LC droplets with a nonuniform surface anchoring are precisely Janus particles [55, 56] with controllable properties.

6. EXPERIMENTAL VERIFICATION

In this section, we compare the results of theoretical and experimental data for the small-angle structure of light scattered by a PDLC monolayer that consists of polydisperse spheroidal LC droplets with a uniform tangential anchoring and bipolar intrinsic configuration of the local director. To compare the results, we have used experimental dependences $I_{vv}^{\text{inc}}(\theta_s)$ and $I_{vh}^{\text{inc}}(\theta_s)$ of the intensity of light scattered in a monolayer PDLC film for the incident light polarization angle $\alpha = 0$ and the angle of orientation of scattering plane $\varphi_s = 0$. The composite film was prepared based on 5CB nematic LC with refractive indices $n_\perp = 1.531$ for the ordinary wave and $n_\parallel = 1.717$ for the extraordinary wave at wavelength $\lambda = 0.633$ μm [44]. The refractive index of the polymer in the prepared sample was $n_p = 1.522$. The filling factor was $\eta = 0.23$. The optical axes of LC droplets were predominantly in the plane of the monolayer PDLC film, and their orientation in the plane of the film was chaotic ($\varphi_m = \pi$) in relations (41)–(47)). The mean diameter of droplet cross sections in the plane of the film was 13.5 μm (the values of the droplet diameter in the sample varied from 6 to 20 μm). The number of LC droplets with a diameter of the cross section in the range 13.5 ± 2.5 μm was about 73% of their total number. The oblateness of the droplets (shape anisometry parameter ε) was approximately 0.7.

In our experiments, a nonpolarized beam from a He–Ne laser (LASOS, $\lambda = 632.8$ nm) passed through the polarizer and was incident along the normal to the sample surface. Scattered light passing through the analyzer and the diaphragm was registered by a photodetector. The diaphragm size was chosen for averaging the speckle structure and for measuring the angular distribution of the scattered light intensity components with a small aperture angle of detection.

The experimental and calculated dependences for components $I_{vv}^{\text{inc}}(\theta_s)$ and $I_{vh}^{\text{inc}}(\theta_s)$ of the scattered light intensity are shown in Fig. 4. The calculations were performed using above expressions (48)–(58) and (62) on the basis of the substitution model (relations (36)–(47)). In numerical calculations, polydispersity of LC droplets was taken into account using the measured histogram of the distribution for radius *c* of the LC droplet cross section and for the same value of anisometry parameter $\varepsilon = 0.7$. Figure 4 clearly shows good agreement between the experimental and theoretical data.

7. NUMERICAL ANALYSIS OF THE SMALL-ANGLE DISTRIBUTION OF SCATTERED LIGHT INTENSITY: ASYMMETRY EFFECT

In this section, we consider the results of calculations that illustrate the variations in the structure of radiation scattered into small angles by an individual LC droplet depending on its size, anisometry, and intrinsic configuration of the director field. We analyze the effect of orientation angle φ_s of the polarization plane and polarization angle α of incident light on the characteristics of scattered radiation. For monolayer PDLC films, we analyze the effect of sizes, polydispersity, and concentration of LC droplets on the angular distribution of the scattered light intensity. We also analyze the effect of asymmetry [27–29] of the small-angle distribution of the scattered light intensity over scattering angle θ_s (the essence of this effect was described in Introduction). It will be shown that the polydispersity of LC droplets and disorientation of their optical axes do not suppress the asymmetry effect. Main attention will be paid to analyzing the

vv component of scattered light intensity I_{vv}^{inc}. For the vh component I_{vh}^{inc}, analogous qualitative tendencies are observed.

The $I_{vv,vh}^{c}$ components of the intensity of radiation scattered by an individual LC droplet can be determined using the relations

$$I_{vv,vh}^{s}(\theta_s, \varphi_s) = C\frac{1}{\sigma k^2}|f_{vv,vh}(\theta_s, \varphi_s)|^2, \qquad (63)$$

which follow from expressions (2) for the scattered field in the far wave zone. In expression (63), normalization constant C is defined in the same way as in expression (32); the components $f_{vv,\,vh}(\theta_s, \varphi_s)$ of the vector amplitude scattering function (expressions (33), (34)) are determined using relations (48)–(51) for the amplitude scattering matrix elements $S_j(\theta_s, \varphi_s), j = 1, 2, 3, 4$.

Figure 5a shows the I_{vv}^{s} component of the intensity of radiation scattered by an individual spherical droplet of radius $c = 5$ μm for zero values of polarization angle α and scattering angle φ_s. The calculations were carried out for different values of parameter w (see Section 5) characterizing the fraction of the normal and tangential anchoring. All calculations were performed for 5CB LC ($n_\perp = 1.531$, $n_\parallel = 1.717$; $\lambda = 0.633$ μm).The refractive index of the polymer matrix was assumed to be equal to the refractive index of the ordinary wave in the LC ($n_p = n_\perp$).

It can be seen from Fig. 5a that, for $w = 0$ and 100%, the angular distribution of the scattered light intensity is symmetric in scattering angle θ_s relative to the strictly forward direction of scattering ($\theta_s = 0$). These conditions ($w = 0$ and 100%) correspond to uniform surface anchoring for droplets with bipolar and radial configurations of local director $\mathbf{n}(\mathbf{r})$. In the case of nonuniform anchoring, for $w = 25$, 50, and 75%, we observe a shift in the positions of main peaks in the angular distribution of scattered radiation intensity relative to direction $\theta_s = 0$ and asymmetric arrangement of other peaks; i.e., asymmetry effect in the scattered light intensity distribution in scattering angle θ_s is observed. The strongest displacement of the main peak is observed for $w = 50$%, i.e., when the fraction of normal and tangential boundary conditions on the surface of an LC droplet are identical.

Figure 5b illustrates the asymmetry contrast K_a. We define it as the ratio of the difference of intensities $I_{vv}^{s}(\theta_s) - I_{vv}^{s}(-\theta_s)$ to their sum $I_{vv}^{s}(\theta_s) + I_{vv}^{s}(-\theta_s)$. For homogeneous boundary conditions ($w = 0$ and 100%), it is equal to zero, while for inhomogeneous conditions, it varies from −1 to +1. Negative values of the contrast correspond to stronger scattering to the left from the strictly forward direction, while positive values correspond to stronger scattering to the right, where normal boundary conditions are observed.

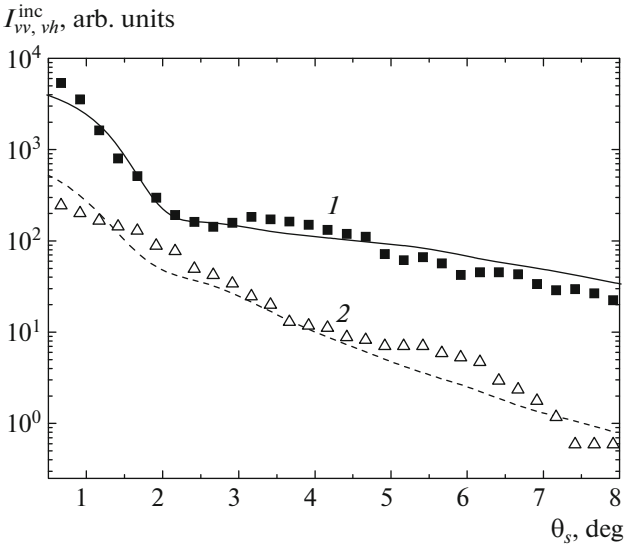

Fig. 4. Theoretical (curves) and experimental (symbols) dependences of components I_{vv}^{inc} (*1*) and I_{vh}^{inc} (*2*) of the intensity of light scattered by the PDLC monolayer on the scattering angle θ_s for $\alpha = 0$, $\varphi_s = 0$, $n_\parallel = 1.717$, $n_\perp = 1.531$ ($\lambda = 0.633$ μm), $n_p = 1.522$, and $\eta = 0.23$.

Figure 6 shows scattered light intensity component $I_{vv}^{s}(\theta_s)$ for $w = 50$% and different values of φ_s and α. Figure 6a illustrates the angular structure of scattered light intensity for zero polarization angle ($\alpha = 0$). It can be seen that (i) the asymmetry effect disappears for $\varphi_s = 45°$, 90°, and 135°; (ii) intensity curves $I_{vv}^{s}(\theta_s)$ for $\varphi_s = 45°$ and $\varphi_s = 135°$ coincide; (iii) the $I_{vv}^{s}(\theta_s)$ curves for $\varphi_s = 0$ and $\varphi_s = 180°$ are specularly symmetric relative to the strictly forward direction of scattering ($\theta_s = 0$). These results are a consequence of the symmetry properties of the internal structure of an LC droplet for $w = 50$% and nonequivalence of the +**N** and −**N** directions for the optical axis of the droplet with nonuniform anchoring.

A slightly different situation (Fig. 6b) takes place for different values of polarization angle α and a constant angle φ_s: the asymmetry effect is observed for $\alpha = 45°$ and 135° and disappears only for $\alpha = 90°$. For $\alpha = 0$ and 180°, the $I_{vv}^{s}(\theta_s)$ curves coincide and are not specularly symmetric.

The effect of the size of spherical droplets and of anisometry parameter for spheroids oblate in the direction of light incidence on the angular structure of the vv component of the scattering light intensity is illustrated in Figs. 7a and 7b, respectively. It can be seen that no clearly manifested tendency in the enhancement or suppression of the scattering asymmetry effect is observed with decreasing droplet radius c (for spheres) or anisometry parameter ε (for

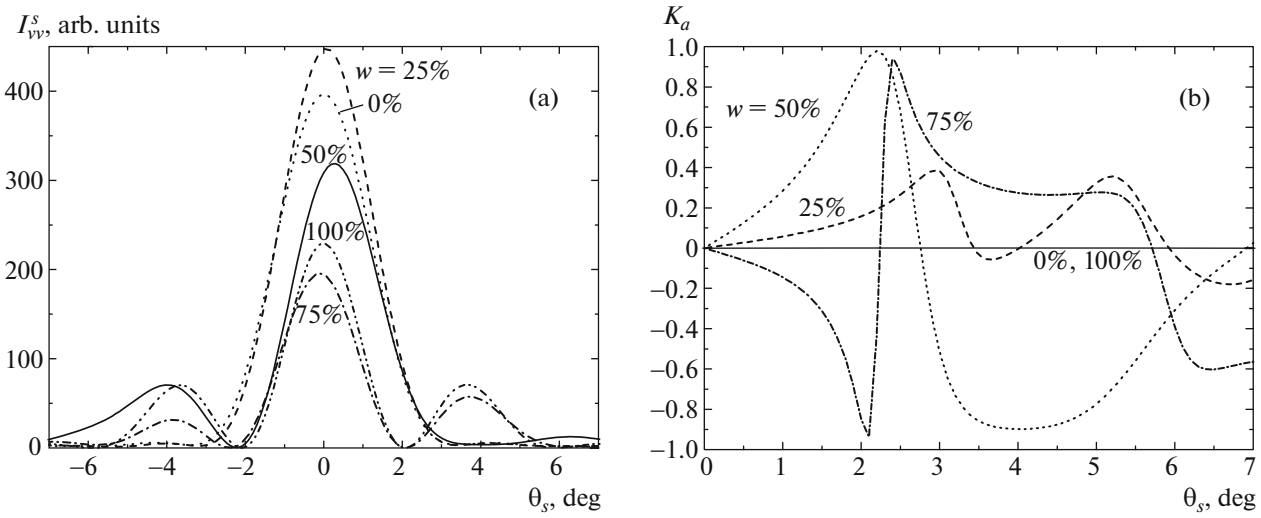

Fig. 5. Dependences of (a) scattered light intensity component I^s_{vv} and (b) of asymmetry contrast K_a on scattering angle θ_s for a spherical LC droplet with uniform and nonuniform anchoring for different values of parameter w. Droplet radius $c = 5$ μm, $\varphi_s = 0$, $n_\parallel = 1.717$, $n_\perp = 1.531$ ($\lambda = 0.633$ μm), $n_p = n_\perp$.

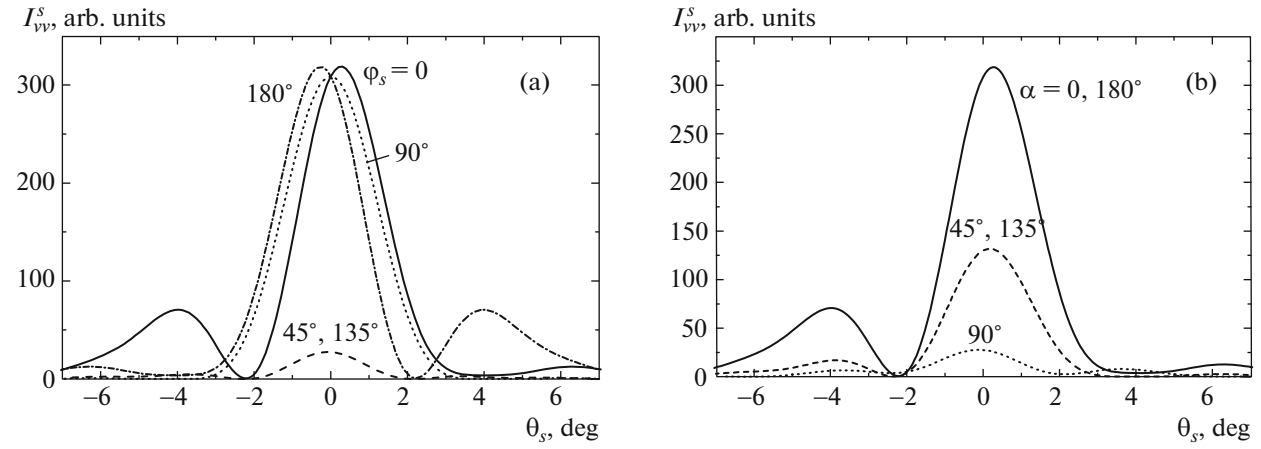

Fig. 6. Components $I^s_{vv}(\theta_s)$ of intensity of light scattered by a spherical LC droplet for (a) different values of angle φ_s of orientation of the scattering plane and (b) different values of polarization angle α of incident light for $\varphi_s = 0$. Droplet radius $c = 5$ μm, parameter $w = 50\%$, $n_\parallel = 1.717$, $n_\perp = 1.531$ ($\lambda = 0.633$ μm), $n_p = n_\perp$.

spheroids). The effect is weaker in some cases and stronger in other cases. In the ranges of sizes and anisometry of a LC droplet in the anomalous diffraction approximation considered here, the asymmetry effect is manifested most clearly for a spherical droplet with radius $c = 5$ μm. It can also be seen from Fig. 7a that, with the decreasing size (radius c) of an LC droplet, the $I^s_{vv}(\theta_s)$ component of the scattered light intensity becomes more diffusive as expected [32, 45]. As can be seen from Fig. 7b, a decrease in anisometry parameter ε for $\varepsilon < 0.7$ conversely leads to the elongation of the scattering indicatrix in the forward direction.

Thus, the main reason for the small-angular scattering asymmetry effect is the nonuniformity of surface anchoring of an LC droplet with the polymer matrix. The extent of the manifestation of this effect depends on the size of the droplet, anisometry of its shape, and conditions illumination and observation of scattered light. This effect is of the interference origin and can be explained on the basis of the Huygens–Fresnel principle [31] if we consider an LC droplet to be a flat screen (Fig. 8).

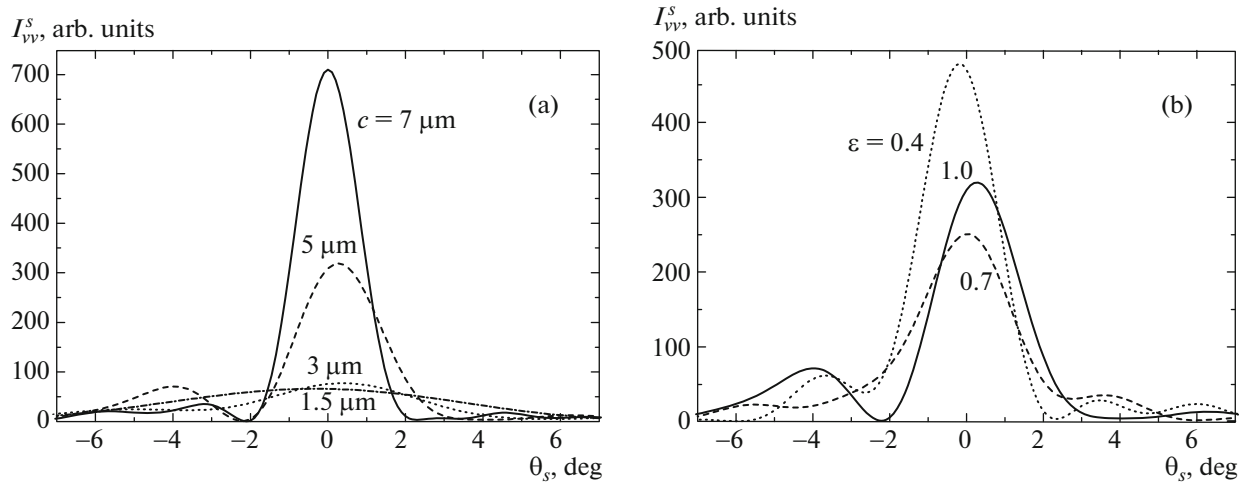

Fig. 7. Influence of (a) spherical LC droplet radius c and (b) anisometry parameter ε of a spheroidal LC droplet with $c = 5$ μm on the asymmetry of angular distribution $I^s_{vv}(\theta_s)$ of the scattered light intensity component: $w = 50\%$, $\alpha = 0$, $\varphi_s = 0$, $n_\parallel = 1.717$, $n_\perp = 1.531$ ($\lambda = 0.633$ μm), $n_p = n_\perp$.

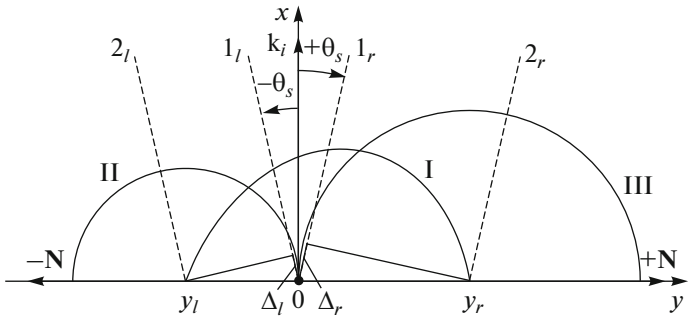

Fig. 8. Schematic diagram of the xy section of a droplet for explaining the asymmetry effect in scattering of the extraordinary wave with the y polarization ($w = 50\%$); $\mathbf{k}_i$ is the wavevector of the incident wave; $-\theta_s$ and θ_s are the scattering angle relative to the direction of incidence of light. The fronts of secondary waves emerging from the points with coordinates $y = 0$, $y = y_l$, and $y = y_r$ are denoted by Roman numbers I, II, and III.

Figure 8 shows the geometry for a droplet with $w = 50\%$, which explains the scattering asymmetry for the extraordinary wave with the y polarization. The figure shows three fronts of secondary waves that emerge from points with coordinates $y = 0$, $y = y_l$, and $y = y_r$, respectively, from the center of the droplet on the left and right of the xy plane dividing the droplet into regions with tangential and normal surface anchoring. The front of the secondary wave for the point with coordinate $y = 0$ is not spherical in view of the difference in the refractive indices of the LC droplet for $y < 0$ and $y > 0$. In a certain time interval Δt, the front reaches coordinates y_l and y_r, which are not equal in absolute values. Over the same time interval, spherical fronts of the secondary waves emerging from points y_l and y_r are formed. As can be seen from Fig. 8, phases differences Δ_l and Δ_r for the wave normals along lines 1_l, 2_l and 1_r, 2_r (on the left and right of the x axis) for angles $-\theta_s$ and θ_s are different ($\Delta_l \neq \Delta_r$). As a result of interference of secondary waves 1_l with 2_l and 1_r with 2_r, the corresponding intensities $I(-\theta_s)$ and $I(\theta_s)$ are also different.

Figure 9 illustrates scattering of light by an ensemble of LC droplets with nonuniform anchoring; the results of calculation of the intensity component I^{inc}_{vv} of light scattered by a monolayer monodisperse PDLC film containing spherical LC droplets are plotted for different values of their radius c and layer filling factor η. The calculations were performed using relation (32).

Comparison of Figs. 9a–9c shows that, with increasing concentration of droplets (filling factor η), the asymmetry effect becomes stronger. Under certain conditions determined by the sizes of LC droplets and

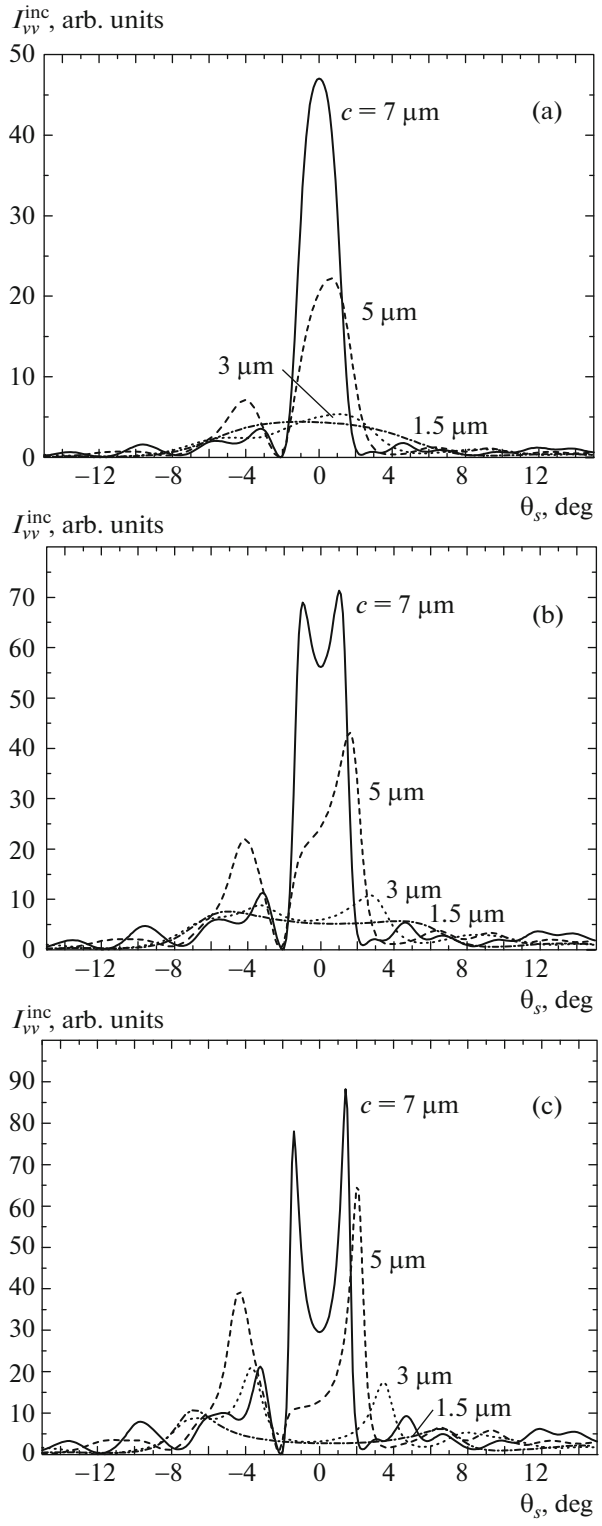

Fig. 9. Components $I_{vv}^{inc}(\theta_s)$ of intensity of light scattered by a PDLC film containing a monolayer of monodisperse LC droplets for different values of their radius c and filling factor η: (a) η = 0.1; (b) η = 0.3; and (c) η = 0.5 for w = 50%, α = 0, φ_s = 0, $n_\parallel$ = 1.717, $n_\perp$ = 1.531 (λ = 0.633 μm), $n_p = n_\perp$.

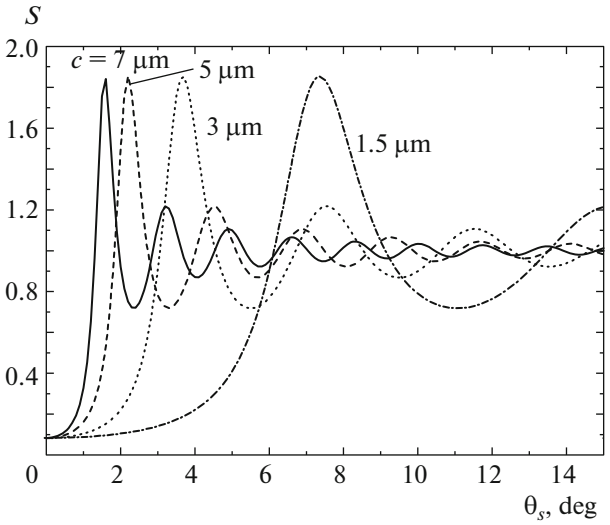

Fig. 10. Structural factor $S(\theta_s)$ of a PDLC monolayer of monodisperse LC droplets for different values of their radius c. Filling factor is η = 0.5.

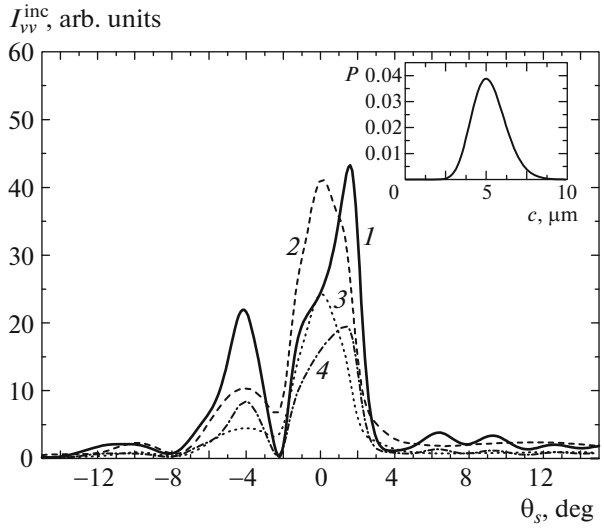

Fig. 11. Effect of polydispersity of LC droplets and disorientation of their optical axes in a PDLC monolayer on the effect of asymmetry in light scattering: (*1*) monolayer of monodisperse LC droplets with oriented optical axes ($D_c/\langle c\rangle = 0$, $\varphi_m = 0$); (*2*) monolayer of monodisperse LC droplets with oriented optical axes ($D_c/\langle c\rangle = 0.2$, $\varphi_m = 0$); (*3*) monolayer of monodisperse LC droplets with oriented optical axes ($D_c/\langle c\rangle = 0.2$, $\varphi_m = 180°$); (*4*) monolayer of monodisperse LC droplets with disoriented optical axes ($D_c/\langle c\rangle = 0$, $\varphi_m = 180°$); w = 50%, α = 0, φ_s = 0, η = 0.3, $n_\parallel$ =1.717, $n_\perp$ = 1.531 (λ = 0.633 μm), $n_p = n_\perp$. Modal radius of droplets c_m = 5 μm. The inset shows probability density P of the distribution of LC droplets over radius c used in calculations (gamma distribution) for $D_c/\langle c\rangle = 0.2$, c_m = 5 μm.

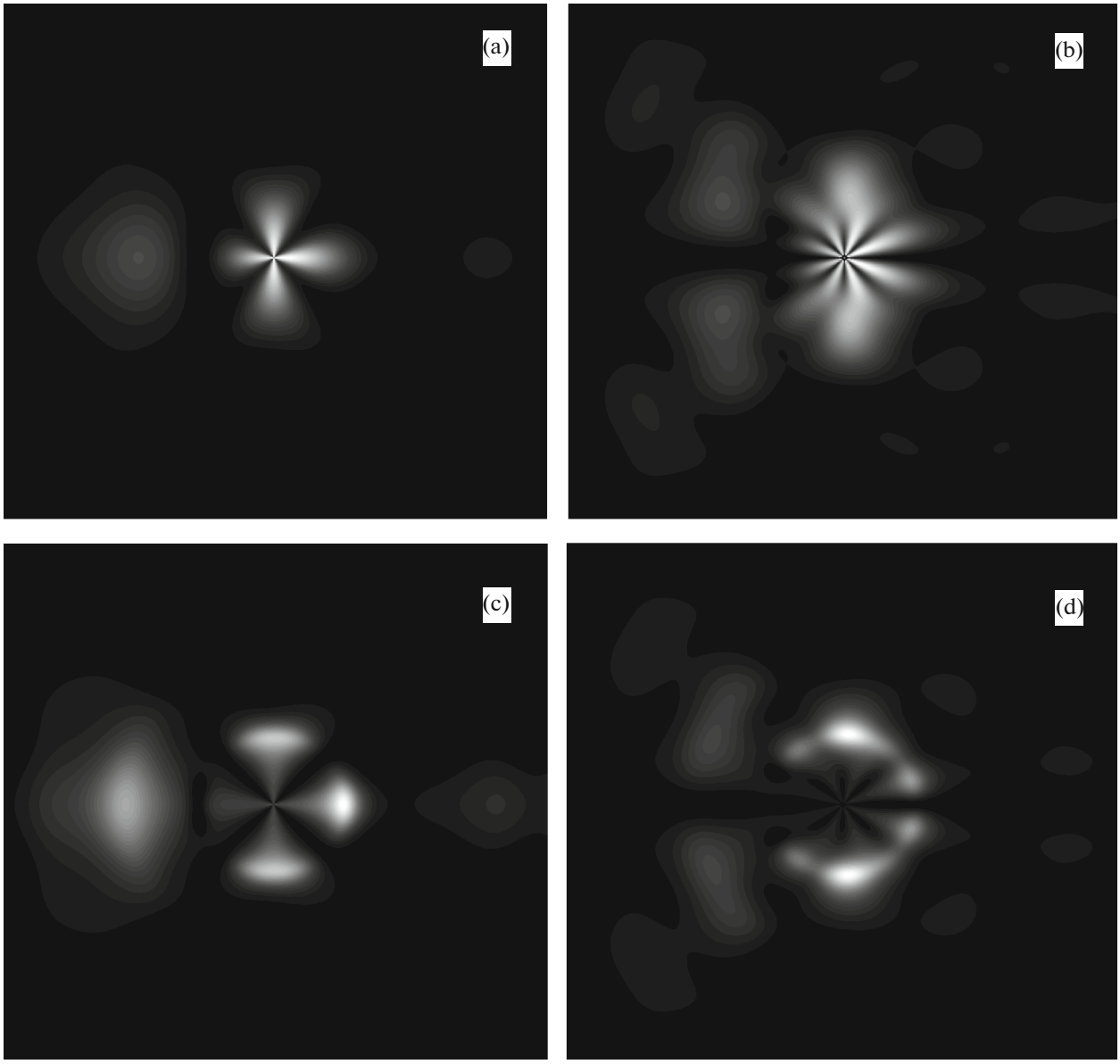

Fig. 12. Angular distributions of components (a) $I^{s}_{vv}(\theta_s, \varphi_s)$ and (b) $I^{s}_{vh}(\theta_s, \varphi_s)$ of intensity of light scattered by an individual LC droplet, as well as (c) $I^{\text{inc}}_{vv}(\theta_s, \varphi_s)$ and (d) $I^{\text{inc}}_{vh}(\theta_s, \varphi_s)$ of the intensity of light scattered by a PDLC monolayer of monodisperse LC droplets. Filling factor $\eta = 0.5$. Droplet radius $c = 5$ μm, $\alpha = 0$, $w = 50\%$, $n_{\parallel} = 1.717$, $n_{\perp} = 1.531$ ($\lambda = 0.633$ μm), $n_p = n_{\perp}$.

their concentration, it becomes more clearly manifested. This is a consequence of the manifestation of interference effects in light scattering by the ensemble of LC droplets in the film. The intensity of the redistribution of the scattered light due to interference, which determines the extent of manifestation of the asymmetry effect in scattering by the PDLC monolayer, depends on structural factor S (see Section 2). For a monolayer of monodisperse droplets, it is described by relation (31) and is illustrated in Fig. 10. It can be seen from the figure that the number of oscillations of function $S(\theta_s)$ depends on the size of LC droplets, which in turn determines the number of asymmetric maxima and minima on the $I^{\text{inc}}_{vv}(\theta_s)$ curve for different sizes of droplets.

The effect of polydispersity of droplets and disorientation of their optical axes on the angular structure of the intensity of light scattered by the PDLC monolayer is illustrated in Fig. 11. The calculations were performed using the substitution model on the basis of relations (36)–(47). The polydispersity of droplets is taken into account using the gamma distribution [30] of probability density $P(c)$ of droplets over radius c as follows:

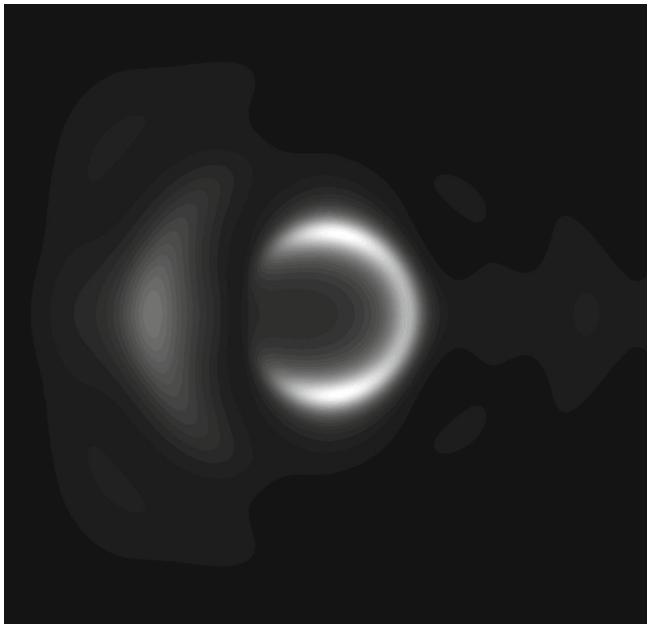

Fig. 13. Angular distribution $I_{np}(\theta_s, \varphi_s)$ of the intensity of light scattered by a PDLC monolayer of monodisperse spherical LC droplets under illumination by nonpolarized radiation. Filling factor $\eta = 0.5$. Droplet radius $c = 5$ μm, $w = 50\%$, $n_\parallel = 1.717$, $n_\perp = 1.531$ ($\lambda = 0.633$ μm), $n_p = n_\perp$.

$$P(c) = \frac{\mu^{\mu+1}}{\Gamma(\mu+1)}\frac{c^\mu}{c_m^{\mu+1}}\exp\left(-\frac{\mu c}{c_m}\right), \quad (64)$$

where μ is the parameter of the distribution, Γ is the gamma function, and c_m is the modal (most probable) droplet radius. Modal radius c_m and parameter μ are connected with mean value $\langle c\rangle$ of the radius of droplets and variation coefficient $D_c/\langle c\rangle$, respectively, where D_c is the standard (mean-square) deviation as follows:

$$c_m = \frac{\mu}{\mu+1}\langle c\rangle, \quad (65)$$

$$\mu = 1/(D_c/\langle c\rangle)^2 - 1. \quad (66)$$

Figure 11 shows the results of calculation of $I_{vv}^{\text{inc}}(\theta_s)$ for PDLC monolayers that contain monodisperse and polydisperse droplets for $c_m = 5$ μm and for different variations in the optical axes of the droplets, which are determined by angle φ_m (see Section 3).

It can be seen from the results of calculations that the polydispersity of droplets and the disorientation of their optical axes do not lead to disappearance of the effect of asymmetry of light scattering under investigation. This is due to the fact that directions +**N** and −**N** of the optical axis of a droplets with nonuniform anchoring are not equivalent.

The asymmetry effect considered here is visually illustrated in Figs. 12 and 13. Figures 12a and 12b show components $I_{vv}^{s}(\theta_s, \varphi_s)$ and $I_{vh}^{s}(\theta_s, \varphi_s)$ of the intensity of light scattered by an individual LC droplet (expression (63)) for scattering angles $-8° \le \theta_s \le 8°$ and $0 \le \varphi_s \le 180°$ in the case when the layer is illuminated by polarized radiation with polarization angle $\alpha = 0$. Brighter regions in the figures correspond to higher intensities. The *y* axis of the laboratory system of coordinates is directed along the horizontal, while the *z* axis is directed along the vertical. The calculations were performed for $w = 50\%$ and $n_p = n_\perp$ for 5CB LC.

Figures 12c and 12d show components $I_{vv}^{\text{inc}}(\theta_s, \varphi_s)$ and $I_{vh}^{\text{inc}}(\theta_s, \varphi_s)$ of the intensity of light scattered by the PDLC monolayer (expressions (32)) for filling factor $\eta = 0.5$. It can be seen that, in contrast to uniform anchoring [43, 57], no central symmetry is observed in the angular structure of radiation scattered by the layer with nonuniform interfacial anchoring.

The asymmetry effect is also manifested when a PDLC monolayer with nonuniform interface anchoring is illuminated by nonpolarized monochromatic radiation (Fig. 13). Figure 13 shows the intensity $I_{np}(\theta_s, \varphi_s)$ of scattered radiation for nonpolarized incident light,

$$I_{np}(\theta_s, \varphi_s) = \frac{1}{2}[(I_{vv}^{\text{inc}}(\theta_s, \varphi_s) + I_{vh}^{\text{inc}}(\theta_s, \varphi_s))_{\alpha=0} + (I_{vv}^{\text{inc}}(\theta_s, \varphi_s) + I_{vh}^{\text{inc}}(\theta_s, \varphi_s))_{\alpha=\pi/2}]. \quad (67)$$

This relation was obtained from expression (32) by averaging over polarization angle α with a uniform distribution in the range from 0 to 2π. The values of $I_{np}(\theta_s, \varphi_s)$ shown in Fig. 13 were calculated for the same parameters as for $I_{vv,vh}^{\text{inc}}(\theta_s, \varphi_s)$ shown in Figs. 12c and 12d.

8. CONCLUSIONS

We have developed the methods for the description and numerical simulation of the angular distribution of the intensity of radiation scattered by a PDLC monolayer with uniform and nonuniform interfacial anchoring using the interference approximation. We have considered the results of calculations that illustrate the change in the structure of radiation scattered within small angles that depend on the internal structure of LC droplets, their concentration, sizes, polydispersity, and anisometry. We have analyzed the intensity of scattered light depending on the conditions of illumination and detection of scattered light.

The methods developed here have been verified experimentally.

We have demonstrated the possibility of realizing the electrooptical effect of asymmetry in the small-angle structure of light scattered in the PDLC monolayer with nonuniform interfacial boundary conditions.

The results of this study can be used in developing electrooptical devices based on LC films dispersed by a polymer (amplitude and phase modulators of light, polarization transformers, displays, etc.) in which the optical response is determined by the variations in the LC configuration under the action of external factors. In particular, these results are applicable in designing devices for masking optical information.

ACKNOWLEDGMENTS

This work was performed under the interacademic integration project between the National Academy of Sciences of Belarus and the Siberian Branch of the Russian Academy of Sciences and supported by the Belarus Republic Foundation for Fundamental Research (project no. F15SO-039). One of the authors (V.Ya.Z.) thanks the Russian Foundation for Basic Research and the Administration of the Krasnoyarsk Territory (project no. 16-42-240704).

REFERENCES

1. G. M. Zharkova and A. S. Sonin, *Liquid Crystal Composites* (Nauka, Moscow, 1994) [in Russian].
2. F. Simoni, *Nonlinear Properties of Liquid Crystals and Polymer Dispersed Liquid Crystals* (World Scientific, Singapore, 1997).
3. M. G. Tomilin and S. M. Pestov, *Properties of Liquid Crystal Materials* (Politekhnika, St. Petersburg, 2005) [in Russian].
4. *Display Systems*, Ed. by L. W. MacDonald and A. C. Lowe (Wiley, New York, 1997).
5. V. G. Chigrinov, *Liquid Crystal Devices: Physics and Application* (Artech House, Boston, 1999).
6. V. Ya. Zyryanov, S. L. Smorgon, and V. F. Shabanov, Mol. Eng. **1**, 305 (1992).
7. F. Basile, F. Bloisi, L. Vicari, and F. Simoni, Phys. Rev. E **48**, 432 (1993).
8. V. V. Presnyakov and T. V. Galstian, Mol. Cryst. Liq. Cryst. **413**, 435 (2004).
9. V. A. Loiko and A. V. Konkolovich, J. Exp. Theor. Phys. **96**, 489 (2003).
10. V. A. Loiko and A. V. Konkolovich, J. Exp. Theor. Phys. **99**, 343 (2004).
11. V. A. Loiko and A. V. Konkolovich, J. Exp. Theor. Phys. **103**, 935 (2006).
12. P. G. Lisinetskaya, A. V. Konkolovich, and A. V. Loiko, Appl. Opt. **48**, 3144 (2009).
13. A. Khan, I. Shiyanovskaya, T. Schneider, et al., J. SID **15**, 9 (2007).
14. G. E. Volovik and O. D. Lavrentovich, Sov. Phys. JETP **58**, 1159 (1983).
15. P. S. Drzaic, *Liquid Crystal Dispersions* (World Sci., Singapore, 1995).
16. J. L. West, J. W. Doane, and S. Zumer, US Patent No. 4685771, Int. Cl. G02F 1/13 (1987).
17. V. K. Freedericksz and V. Zolina, Trans. Faraday Soc. **29**, 919 (1933).
18. V. Ya. Zyryanov, M. N. Krakhalev, O. O. Prishchepa, and A. V. Shabanov, JETP Lett. **86**, 383 (2007).
19. E. Dubois-Violette and P. G. de Gennes, J. Phys. Lett. **36**, L-255 (1975).
20. L. M. Blinov, E. I. Kats, and A. A. Sonin, Sov. Phys. Usp. **30**, 604 (1987).
21. S. Zumer and J. W. Doane, Phys. Rev. A **34**, 3373 (1986).
22. S. Zumer, Phys. Rev. A **37**, 4006 (1988).
23. D. A. Yakovlev and O. A. Afonin, Opt. Spectrosc. **82**, 78 (1997).
24. V. A. Loiko, P. G. Maksimenko, and A. V. Konkolovich, Opt. Spectrosc. **105**, 791 (2008).
25. V. A. Loiko, A. V. Konkolovich, and A. A. Miskevich, J. Exp. Theor. Phys. **122**, 176 (2016).
26. V. A. Loiko, V. Ya. Zyryanov, A. V. Konkolovich and A. A. Miskevich, Opt. Spectrosc. **120**, 143 (2016).
27. V. A. Loiko, U. Mashke, V. Ya. Zyryanov, A. V. Konkolovich, and A. A. Miskevich, Opt. Spectrosc. **111**, 866 (2011).
28. V. A. Loiko, V. Ya. Zyryanov, U. Maschke, et al., J. Quant. Spectrosc. Rad. Transfer **113**, 2585 (2012).
29. V. A. Loiko, V. Ya. Zyryanov, A. V. Konkolovich, et al., Mol. Cryst. Liq. Cryst. **561**, 194 (2012).
30. V. A. Loiko and A. V. Konkolovich, J. Phys. D **33**, 2201 (2000).
31. M. Born and E. Wolf, *Principles of Optics* (Pergamon, Oxford, 1964; Nauka, Moscow, 1970).
32. C. Bohren and D. Huffman, *Absorption and Scattering of Light by Small Particles* (Wiley, New York, 1998; Mir, Moscow, 1986).
33. V. I. Iveronova and G. P. Revkevich, *Theory of X-ray Scattering* (Mosk. Gos. Univ., Moscow, 1978) [in Russian].
34. A. P. Ivanov, V. A. Loiko, and V. P. Dik, *Light Propagation in Densely Packed Dispersed Media* (Nauka Tekhnika, Minsk, 1988) [in Russian].
35. J. Ziman, *Models of Disorder: The Theoretical Physics of Homogeneously Disordered Systems* (Cambridge Univ., Cambridge, 1979; Mir, Moscow, 1982).
36. M. S. Wertheim, Phys. Rev. Lett. **10**, 321 (1963).
37. Y. Rosenfeld, Phys. Rev. A **42**, 5978 (1990).
38. K. H. Ding, C. E. Mandt, L. Tsang, and J. A. Kong, J. Electromagn. Waves Appl. **6**, 1015 (1992).
39. K. M. Hong, J. Opt. Soc. Am. **70**, 821 (1980).
40. *Scattering of Electromagnetic Waves: Numerical Simulations*, Ed. by J. Kong (Wiley, New York, 2001).
41. J. A. Lock and Chiu Chin-Lien, Appl. Opt. **33**, 4663 (1994).
42. V. A. Loiko and A. V. Konkolovich, Opt. Spektrosc. **85**, 623 (1998).
43. V. A. Loiko, U. Mashke, V. Ya. Zyryanov, et al., Opt. Spektrosc. **110**, 116 (2011).
44. V. A. Loiko, M. N. Krakhalev, A. V. Konkolovichet al., J. Quant. Spectrosc. Radiat. Transfer **178**, 263 (2016).
45. H. C. van de Hulst, *Light Scattering by Small Particles* (Dover, New York, 1981; Inostr. Liter., Moscow, 1961).
46. V. N. Lopatin and N. V. Shepelevich, Opt. Spectrosc. **81**, 103 (1996).

47. G. H. Meeten, Opt. Acta **29**, 759 (1982).
48. R. Azzam and N. Bashara, *Ellipsometry and Polarized Light* (North-Holland, Amsterdam, 1977; Mir, Moscow, 1981).
49. E. V. Ishchenko and A. L. Sokolov, *Polarization Optics* (Mosk. Energet. Inst., Moscow, 2005) [in Russian].
50. L. M. Blinov, *Structure and Properties of Liquid Crystals* (Springer, New York, 2011).
51. O. O. Prischepa, A. V. Shabanov, and V. Ya. Zyryanov, JETP Lett. **79**, 257 (2004).
52. O. O. Prishchepa, A. V. Shabanov, and V. Ya. Zyryanov, Phys. Rev. E **72**, 031712 (2005).
53. V. Ya. Zyryanov, M. N. Krakhalev, and O. O. Prishchepa, Mol. Cryst. Liq. Cryst. **489**, 273 (2008).
54. V. Ya. Zyryanov, M. N. Krakhalev, O. O. Prishchepa, and A. V. Shabanov, JETP Lett. **88**, 597 (2008).
55. A. Walther and A. Muller, Soft Matter **4**, 663 (2008).
56. A. Perro, S. Reculusa, S. Ravaine, et al., J. Mater. Chem. **15**, 3745 (2005).
57. V. A. Loiko, U. Mashke, V. Ya. Zyryanov, A. V. Konkolovich, and A. A. Misckevich, J. Exp. Theor. Phys. **107**, 692 (2008).

Translated by N. Wadhwa